

Optimal time for sensing in open quantum systems

Zain H. Saleem*

Mathematics and Computer Science Division, Argonne National Laboratory, 9700 S Cass Ave, Lemont IL 60439

Anil Shaji†

School of Physics, IISER Thiruvananthapuram, Kerala, India 695551

Stephen K. Gray‡

Center for Nanoscale Materials, Argonne National Laboratory, Lemont, Illinois 60439, USA

(Dated: October 21, 2022)

We study the time-dependent quantum Fisher Information (QFI) in an open quantum system satisfying the Gorini-Kossakowski-Sudarshan-Lindblad master equation and demonstrate that the conventional definition of the QFI can fail to correlate with the system dynamics. A modified form of the QFI is proposed that is shown to be superior and allows us to determine the optimal time for sensing in these open quantum systems. We also study the dynamics of the system from an effective non-Hermitian dynamics standpoint and use it to understand the scaling of quantum Fisher information when multiple entangled probes are used.

I. INTRODUCTION

The quest for better precision in the estimation of parameters is common to many areas of science ranging from probing or sensing weak electric and magnetic fields, temperature, pressure, and small rotations and displacements, to high-resolution spectroscopy and magnetic resonance, with applications to atomic clocks, geophysics, medicine, and biology. Fundamental limits of precision have been established, within the realm of classical physics, by Cramér [1], Rao [2], and Fisher [3]. Single parameter estimation procedures involve reading-out the state of a probe, prepared in a convenient initial state, after it has interacted with the system under investigation, and then obtaining from the read-out results, an estimate of the parameter of interest, through some convenient estimator. Through a generalization of the classical framework to quantum mechanics, it has been realized that quantum probes can help in increasing the precision of the estimation. The quantum advantage is typically quantified in terms of the enhanced scaling of the measurement uncertainty as a function of the resources required for the estimation procedure using the quantum probe. Unavoidable interaction between the quantum probe and its environment may reduce or even remove the advantage of using quantum states. This is due to the fragility of quantum resources relevant to metrology like coherence and entanglement in the presence of noisy processes like decoherence, dephasing and diffusion.

Quantum sensing and metrology [4–11] involves the exploration of subtle quantum effects to increase the precision of parameter estimation. Quantum sensors have become one of the most promising applications of quantum

technologies, involving single- or multi-parameter estimation. Here we will use quantum Fisher information (QFI) as a tool to study quantum sensing for open quantum systems. The quantum Fisher information [4] quantifies the theoretical bound on the achievable precision in estimating a parameter using a quantum state as a probe and can be regarded as a performance measure of a quantum system as a quantum sensor. The open quantum systems we will study in this work are dynamic, i.e., evolve with time, and therefore it makes more sense to study the time dependence of the quantum Fisher information. This allows us to also determine the time at which quantum sensing is most efficient.

We consider quantum metrology [9] using two-level systems or qubits. The unitary dynamics of the qubits used as quantum probes is such that it encodes the value of the parameter that is measured. However, in addition to the unitary dynamics we consider a dissipative dynamics as well which drive the probe to a ‘sink’ state that is not useful in the measurement scheme. One such scenario of interest is when the qubit levels are represented by two levels of an atom that couples to a cavity field. The coupling strength between the atom and the cavity, for instance, may be the measured quantity. This, in turn, may be connected to other interesting parameters like the motion of one of the mirrors of an opto-mechanical cavity [12]. Interaction with the cavity typically involves dissipative processes in addition to the coherent one that is used for the probing the strength of the atom-cavity coupling. We therefore have to consider the qubit probes as open quantum systems. The atom-cavity system is particularly interesting in the strong and ultra-strong coupling regimes where the atoms respond collectively to the cavity mode leading to potential quantum advantages in the measurement. However before we can explore such collective couplings in multi-atom cases, the single atom and cavity mode system has to be understood from the point of view of quantum sensing and metrology. The atom-cavity system we have considered is not the only

* zsaleem@anl.gov

† shaji@iisertvm.ac.in

‡ gray@anl.gov

quantum metrology scheme for which the analysis presented below is applicable. Sensing or metrology using superconducting qubits [13], photons [14], electron spins etc, can all be viewed along similar lines. The atom-cavity system should therefore be considered as a placeholder and an illustrative example for the more general results presented in the following.

We study the quantum probes that are also open quantum systems [4] using two different approaches. The first is based on the Gorini-Kosskowski-Sudarshan-Lindblad (GKSL) master equation [15–18] where we assume a Markovian interaction of the probe with its environment and integrate out the degrees of freedom of the environment to derive a dynamical equation for the probe. The second approach is based on a non-Hermitian extension of quantum mechanics [19]. Here the Hamiltonian describing the evolution of the probe is assumed to acquire an anti-Hermitian part which can be associated with dissipative effects. We study the time dependent quantum Fisher information using both approaches. In the latter case we will be dealing with only the two levels of the quantum probe while in the former, a third level will be introduced as a sink which represents the state(s) of the probe that are not useful for the measurement in question. We will show how the two level non-hermitian system can be extended to display the GKSL dynamics.

In the non-Hermitian approach one encounters exceptional points that mark the transition of the Hamiltonian from a PT-symmetric form to one that is not PT-symmetric [20]. Possible quantum advantages in sensing and metrology facilitated by such exceptional points have been of interest recently [21]. Framing the metrology scheme using the non-Hermitian as well as GKSL master equation based approaches also allow us to address the question of metrological advantage around the exceptional points. We find no such advantage at the exceptional point, consistent with several previous studies of related systems [21, 22].

In the absence of dissipation, the QFI for the system we consider increases monotonically with time. This means that the achievable precision in the estimate of the parameter of interest will decrease with increased duration of the measurement. However, when dissipation is present, this is not the case. We find that for the parameter estimation problem we are considering, there is an optimal time at which QFI is largest and consequently one can expect to get best possible measurement precision at this time. With dissipation, it is important to also verify whether the bound on the measurement precision given by the QFI is achievable in practice. In the estimation schemes we consider, the readout of the quantum probe involves measuring in the qubit subspace. Dissipation drives the state of the quantum probe outside this subspace and any practical read-out procedure will bear an overhead corresponding to the cases where the qubit is no longer in the relevant subspace. We propose a modification to the QFI which we label as ‘subspace adapted QFI’ that accounts for this overhead and at the same

time clarifies the behaviour around the exceptional point when the non-Hermitian approach is used.

In section II we will introduce classical and quantum Fisher information. We investigate the time dependent QFI for the open quantum systems via the GKSL formalism in section III. Section IV discusses the system from the non-Hermitian approach. We compare SA-QFI with post selection in the section V. In section VI we study the scaling of the QFI’s with the number of qubits in the system. Finally in section VII we give the conclusions and future directions.

II. QUANTUM FISHER INFORMATION AND PARAMETER ESTIMATION

Let us consider the problem of simultaneously estimating n parameters $\mathbf{x}_i = \{x_1, x_2, \dots, x_n\}$ in a quantum experiment and denote the respective estimators of these parameters by $\hat{\mathbf{x}}_i = \{\hat{x}_1, \hat{x}_2, \dots, \hat{x}_n\}$. The uncertainty in the estimator $\hat{\mathbf{x}}_i$ is quantified by the covariance matrix $\text{Cov}(\hat{\mathbf{x}}_i, \hat{\mathbf{x}}_j)$ and is upper bounded by the quantum Cramer-Rao Bound [23],

$$\text{Cov}(\hat{\mathbf{x}}_i, \hat{\mathbf{x}}_j) \geq \frac{1}{MF_{i,j}} \quad (1)$$

where M stands for the total number of experiments and $F_{i,j}$ is the quantum Fisher information matrix which quantifies the responsiveness of the quantum state of the probe to changes in the measured parameters \mathbf{x}_i . The coefficients of the QFI matrix for a given initial state of the probe given by the density matrix ρ are given by the formulae,

$$F_{i,j} = \text{Tr} \left(L_i \frac{\partial \rho}{\partial x_j} \right), \quad (2)$$

where L_i is the symmetric logarithmic derivative [24] for the parameter x_i and is defined implicitly by,

$$\frac{\partial \rho}{\partial x_i} = \frac{1}{2}(\rho L_i + L_i \rho) \quad (3)$$

Upon writing the density matrix in its eigenbasis $\rho = \sum_a \lambda_a |\lambda_a\rangle \langle \lambda_a|$ and substituting in the above equation we get,

$$L_i = \sum_{\{ab|\lambda_a+\lambda_b \neq 0\}} \frac{2}{\lambda_a + \lambda_b} \langle \lambda_a | \partial_i \rho | \lambda_b \rangle | \lambda_a \rangle \langle \lambda_b |, \quad (4)$$

This formula for the SLD when substituted in (2) gives us the QFI for a mixed state [25],

$$F_{ij} = \sum_{\{ab|\lambda_a+\lambda_b \neq 0\}} F_{ij}(a, b) \quad (5)$$

where,

$$F_{ij}(a, b) = \frac{2\text{Re}[\langle \lambda_a | \partial_i \rho | \lambda_b \rangle \langle \lambda_b | \partial_j \rho | \lambda_a \rangle]}{\lambda_a + \lambda_b}, \quad (6)$$

In the above formula one needs to ensure that the summation is performed only over those eigenvalues for which $\lambda_a + \lambda_b \neq 0$. With a little bit of work one can also show that if we have pure parameterized quantum state $|\psi\rangle := |\psi(\vec{x})\rangle$ then the formula for the QFI matrix becomes,

$$F_{ij} = 4\text{Re}[\langle \partial_i \psi | \partial_j \psi \rangle - \langle \partial_i \psi | \psi \rangle \langle \psi | \partial_j \psi \rangle]. \quad (7)$$

The Fisher information for a particular parameter x_i is defined as $F \equiv F_{i,i}$. Since we will be exclusively considering single parameter estimation we use F for QFI and $F(a, b)$ for the individual elements in the mixed state QFI formula, Eq. (6).

III. GKSL MASTER EQUATION

Let us consider a three-level system with a Hamiltonian in the interaction picture or rotating frame given by,

$$H = \hbar g(|e\rangle\langle f| + |f\rangle\langle e|) + \hbar\Delta(|f\rangle\langle f| - |e\rangle\langle e|) \quad (8)$$

where $|e\rangle$ and $|f\rangle$ are the first two excited states of the system, g is the coupling between these excited states and Δ is the detuning parameter. The third state which is the ‘sink’ $|s\rangle$ enters the dynamics through the GKSL master equation,

$$\dot{\rho} = \frac{1}{i\hbar}[H, \rho] + L_e \rho L_e^\dagger - \frac{1}{2}\{L_e^\dagger L_e, \rho\}. \quad (9)$$

The jump operator describing the dissipation is

$$L_e = \sqrt{\gamma_e}|s\rangle\langle e|$$

and it is responsible for the loss of energy from state $|e\rangle$ to the sink, $|s\rangle$. We note that Eqs. (8) and (9) and non-Hermitian variations have previously been considered by Murch and co-workers [13, 26] as models of a three-level superconducting transmon qubit. Of course, this simple model could also describe many other situations, for example, the single excitation manifold of a two-level qubit coupled to a bosonic cavity in a Jaynes-Cummings model.

It is instructive to connect this model to the physical scenario of estimating the interaction between an atom and a cavity mentioned earlier. Imagine a stream of atoms passing through the cavity one by one. Assume that initially the atom is in a state $|f\rangle$ and that the cavity induces coherent transitions between $|f\rangle$ and another atomic level $|e\rangle$. In the lossless case, the probability of the atom exchanging a photon with the cavity and coming to the state $|e\rangle$ during its transit through the cavity is proportional to the coupling g as well as the detuning Δ . We assume that one of these two is the parameter to be estimated and for simplifying the following discussion we assume that this parameter is g . Once the transit time of the atoms through the cavity is fixed, counting the number of atoms that emerge from the cavity in the states $|e\rangle$ and $|f\rangle$ respectively will yield an estimate of

the value of g . This estimate is, in practice, obtained by performing a straightforward one parameter fit of the observed statistics to the probability of de-excitation of the atom obtained from the atom-cavity interaction model. Let us assume that atomic transitions out of the state $|e\rangle$ to levels other than $|f\rangle$ due to various reasons is the main noise in the system. In order to estimate g in such a scenario with losses, a model that takes into account the relevant noise processes is required. The dissipation operator L_e is introduced to account for this noise. The action of the jump operator, L_e , takes the atom-cavity system from the state $|e\rangle$ to a state $|s\rangle$ which serves as a placeholder for all other atomic states except $|e\rangle$ and $|f\rangle$.

To understand the dynamics described by Eqs. (8) and (9), we start by identifying the three relevant basis states in the Hilbert space of the atom-cavity system as,

$$|s\rangle = \begin{pmatrix} 0 \\ 0 \\ 1 \end{pmatrix} \quad |f\rangle = \begin{pmatrix} 0 \\ 1 \\ 0 \end{pmatrix} \quad |e\rangle = \begin{pmatrix} 1 \\ 0 \\ 0 \end{pmatrix} \quad (10)$$

A. Atomic state excited initially

We assume that the probe starts in the atom excited state $|f\rangle$, i.e., $\rho_{ff}(0) = 1$ to get the following analytical result for the evolution of the elements of the density matrix of the quantum probe:

$$\begin{aligned} \rho_{ff}(t) &= \frac{e^{-\gamma_e t/2}}{\alpha^2} \left[8g^2 + (8g^2 - \gamma_e^2) \cos\left(\frac{\alpha t}{2}\right) + \gamma_e \alpha \sin\left(\frac{\alpha t}{2}\right) \right] \\ \rho_{ee}(t) &= \frac{e^{-\gamma_e t/2}}{\alpha^2} 16g^2 \sin^2\left(\frac{\alpha t}{4}\right) \\ \rho_{ss}(t) &= 1 - \frac{e^{-\gamma_e t/2}}{\alpha^2} \left[16g^2 - \gamma_e^2 \cos\left(\frac{\alpha t}{2}\right) + \gamma_e \alpha \sin\left(\frac{\alpha t}{2}\right) \right] \\ \rho_{fe}(t) &= \rho_{ef}^* = 2ig \frac{e^{-\gamma_e t/2}}{\alpha^2} \left[\gamma_e - \gamma_e \cos\left(\frac{\alpha t}{2}\right) + \alpha \sin\left(\frac{\alpha t}{2}\right) \right] \end{aligned} \quad (11)$$

where $\alpha = \sqrt{16g^2 - \gamma_e^2}$ and all other density matrix components are zero. The expressions for the density matrix elements in Eq. (11) are written suggestively in terms of the parameter α . This is because the point $\alpha = 0$ corresponds to an exceptional point when the same system is described using non-Hermitian quantum mechanics (See Sec. IV). We note here that the limit $\alpha \rightarrow 0$ is well defined for all the components of the density matrix in Eq. (11). We can now compute the QFI for this system with respect to either the coupling g or the detuning Δ using Eq. (5). The QFI corresponding to an estimate of g for different values of the coupling is given

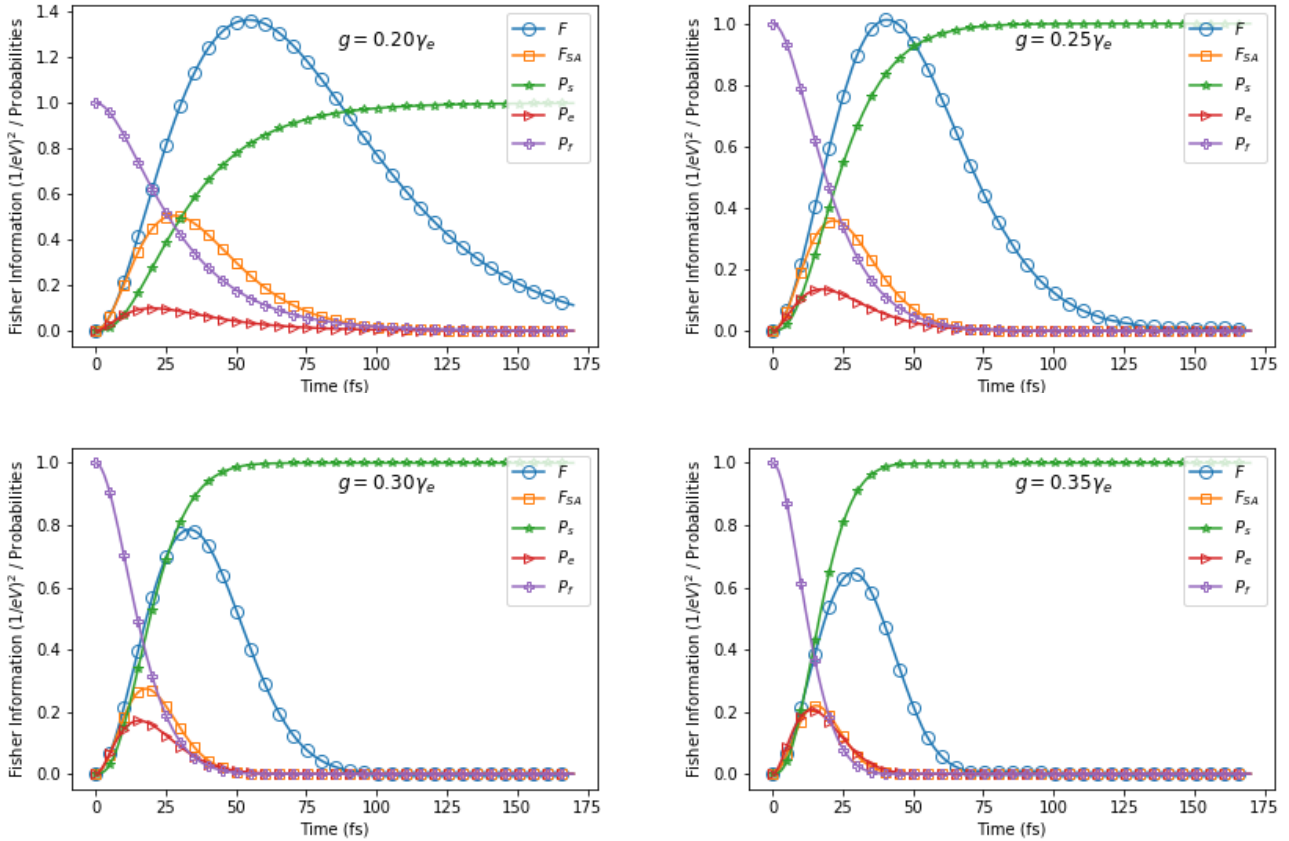


FIG. 1. The Quantum Fisher Information F and the subspace-adapted QFI, F_{SA} corresponding to estimation of the coupling g are plotted as functions of time for different values of g . The initial state of the quantum probe is $|f\rangle$ and the collapse operator used is L_e . The values of g are shown in the respective figures while the other parameters used are: $\hbar\gamma_e = 0.150$ eV and $\hbar\Delta = 0.0$ eV. Also shown in the figures are the density elements ρ_{ee} , ρ_{ff} and ρ_{ss} of the quantum probe. Both the QFI F and SA-QFI, F_{SA} have been scaled-down by a factor of 3000 for displaying on the same scale as the density matrix elements. We see that the peak of F_{SA} appears at a point in time where the probabilities that play a role in estimating g are changing rapidly while the peak of F appears after this dynamics is over.

in Fig. 1. We have also plotted the probabilities for being in different states to understand the correlation of the QFI with the dynamics of the system. We see that the QFI is time-dependent and has a peak at some value in time. This reflects the presence of the noise affecting the estimating process which degrades the sensitivity of the quantum probe with time. In this case, the quantum state of the probe settles down eventually to the state $|s\rangle$ whose evolution at large values of t is not sensitive to changes in g . The low values of QFI for small t is because the probabilities ρ_{ee} , ρ_{ff} and ρ_{ss} are all changing slowly with time reducing their sensitivity to small changes in g . Due to the combined effect of the time taken initially for the QFI to build up and the loss of sensitivity due to noise at later times the QFI has one or more peaks at intermediate times.

B. Subspace-Adapted Quantum Fisher Information

It is tempting to consider the time at which the peak of the QFI occurs as the optimal transit time for the atoms through the cavity since this point appears to furnish maximum sensitivity for the estimation. However, we also see from Fig. 1 that the maximum of the QFI occurs at a point in time when most of the rapid dynamics of the various states has already passed. Examining the expression for QFI in Eq. (5), we see that when ρ_{ff} and ρ_{ee} are both very small for larger values of t the term with $\lambda_e + \lambda_f = \rho_{ff} + \rho_{ee}$ appearing in the denominator can be quite large even if the changes in the corresponding probabilities as a function of g are small. The physical realization of the estimation process we have described makes it clear that the quantum probe will lead to an estimate of g only as long as it remains in the subspace spanned by $|e\rangle$ and $|f\rangle$. If the probe is in the state $|s\rangle$, it is

C. Cavity state excited initially

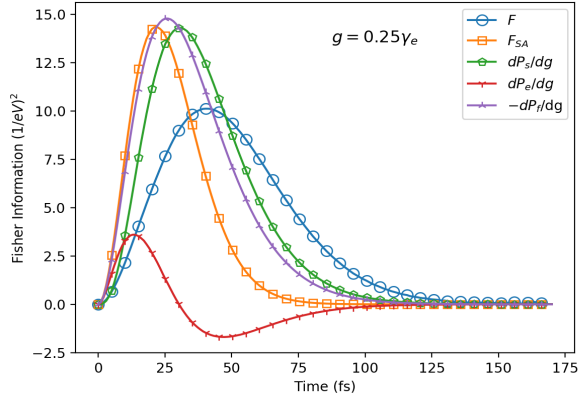


FIG. 2. The parameters in this figure are the same as the top right subfigure in Fig. 1. The QFI and SA-QFI are plotted along with dP_e/dg , dP_f/dg and dP_s/dg versus time. The QFI's have been scaled to fit the scale of the graph and to provide visual ease in seeing the alignment of the QFI's peaks in time with the peaks of the probability derivatives in time. It can be clearly seen that peak in time of SA-QFI better aligns with the points where the rate of change of probabilities with respect to g is the maximum in time.

no longer useful for estimating g . Therefore having $\rho_{ff} + \rho_{ee} \simeq 0$ is not a good operating point for the estimation protocol. In order to get a better guidance for the optimal transit time, we propose a redefinition of the QFI in the presence of the type of losses we have described. Our aim is to find a definition of QFI which fully captures the dynamics of our system. We define a new quantity which we call the Subspace Adapted Quantum Fisher Information (SA-QFI) F_{SA} ,

$$F_{SA} = (\rho_{ee} + \rho_{ff})F \quad (12)$$

and notice from Fig. 1 that the peak of the SA-QFI aligns much better with the point in time where the system is the most dynamic and has maximum sensitivity to g .

Another way to see that SA-QFI better captures the sensitivity of the system to g is by plotting the rate of change of the probabilities P_e , P_f and P_s with respect to g , along with the QFI and SA-QFI against time Fig. 2. We see that the peak of the SA-QFI closely aligns with the point where the rate of change of P_f and P_s with respect to g is the maximum and is also close to the first peak in dP_e/dg . The peak of QFI seems to align with the secondary large magnitude (but a minimum) structure in dP_e/dg . However, at this point in time the probabilities are so small that a much larger number of measurements will be needed to obtain a reliable estimate here. It should be noted that the magnitude of the regular QFI at its maximum in time is higher than the SA-QFI, but that doesn't make its peak the optimal time to perform metrological experiments because of the above mentioned reasons.

To illustrate the usefulness of SA-QFI further as a figure-of-merit for the performance of a quantum sensor in the presence of noise, we consider the case where the atom-cavity system is initialized in the state $|e\rangle$ rather than in the state $|f\rangle$. In this case the detrimental effects of the dissipation start at time $t = 0$ itself. In Fig. 3 we plot the QFI and the SA-QFI along with ρ_{ff} , ρ_{ee} and ρ_{ss} when we initialize the probe in the state $|e\rangle$. We immediately notice that both the QFI's are 10 orders of magnitude smaller compared to the previous case where the system was initialized in $|f\rangle$ suggesting $|e\rangle$ to not be the optimal choice for the initial state for our experiment. In the atom-cavity scenario, this choice corresponds to the atom being in the excited state and it is liable to lose the excitation as a radiated photon at any time during its transit through the cavity without actually depositing the photon in the cavity mode and placing the joint system in the state $|f\rangle$. In the lossless case, estimating the probability of an initially excited atom depositing a photon in the cavity and coming to its unexcited state can equally well serve as a means of estimating g as the case we have already discussed before where the unexcited atom absorbs a photon already present in the cavity. However, our noise model is asymmetric and we have not considered the possibility of loss of the photon from the cavity mode. So having the atom initially in the excited state is not an optimal choice for the measurement as evidenced by the reduced values of the QFI and SA-QFI.

Initializing the probe in state $|e\rangle$ allows for additional interesting features in the QFI. Within the evolution time we have considered in Fig 3, the atom can radiate the photon into the cavity mode and re-absorb it. This is reflected in the small but discernible oscillations between ρ_{ee} and ρ_{ff} at times greater than 50 femtoseconds in Fig. 3. These oscillations are reflected in plot of the QFI as a second peak giving it double peak structure. As pointed out earlier, the large values of QFI at these later times are attributable to the small denominators that appear in Eq. (5) and are in practice not particularly useful because the probability of the quantum probe being in qubit state-space is very small. We see that, on the other hand the SA-QFI has only one clear peak that is sensitive to the dynamics of the system and it successfully discounts the dynamics happening within the qubit subspace when the overall probability of being in that subspace is very low. Note that the peak of SA-QFI shifts its location as we change the value of g . For small values of the coupling, the dynamics in the $|e\rangle$ - $|f\rangle$ subspace is slow and by the time the second exchange of probability between ρ_{ee} and ρ_{ff} happens, the total probability of being in the qubit subspace is negligible. In this case the peak of SA-QFI is shifted to the left where the first exchange between ρ_{ee} and ρ_{ff} occurs. When the coupling is increased the exchange happens sooner and the contribution from it also accounted for. This is reflected

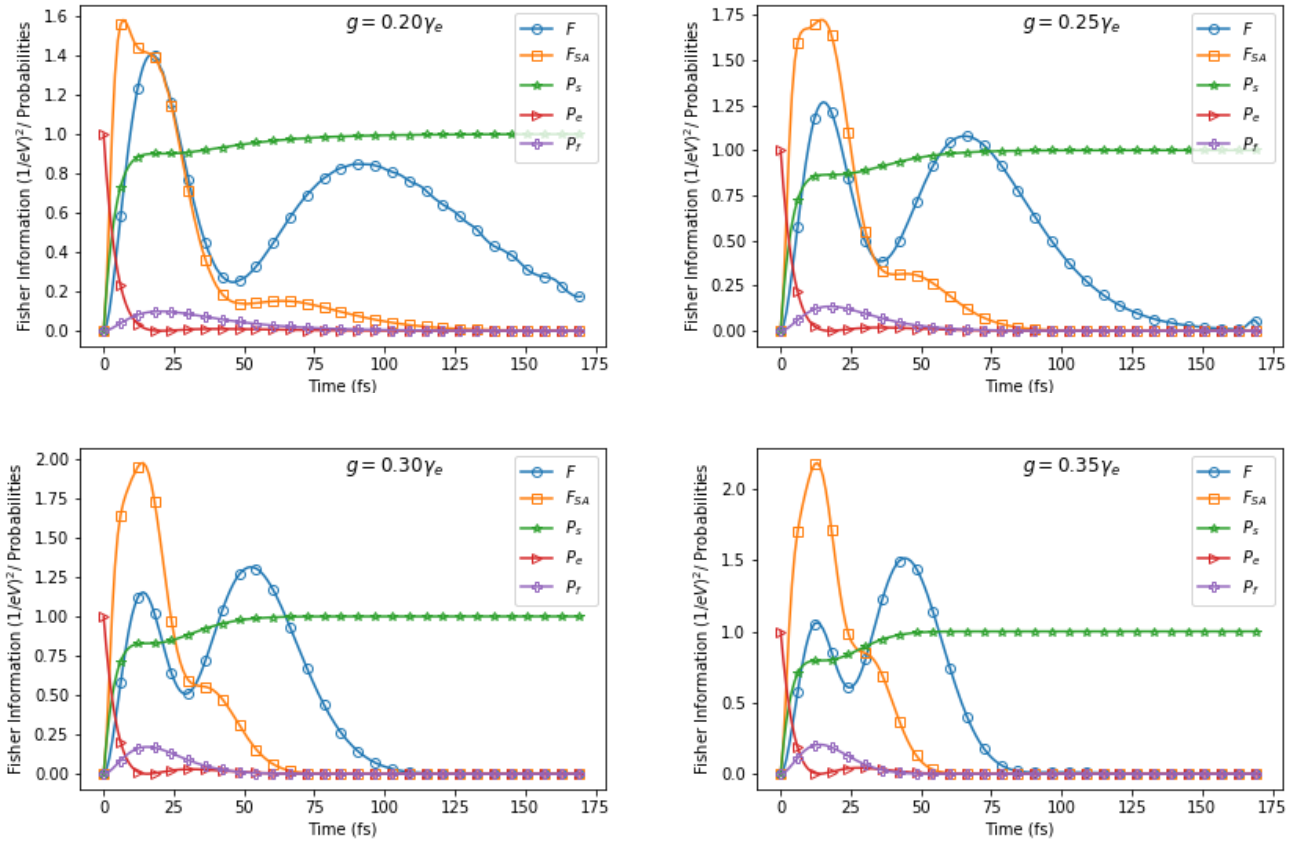


FIG. 3. The QFI F and SA-QFI, F_{SA} corresponding to estimation of the coupling g are plotted as functions of time for different values of g . The initial state of the quantum probe is $|e\rangle$ and the collapse operator used is L_e . The values of g are shown in the respective figures while the other parameters used are: $\hbar\gamma_e = 0.150$ eV and $\hbar\Delta = 0.0$ eV. Also shown in the figures are the density elements ρ_{ee} , ρ_{ff} and ρ_{ss} of the quantum probe. In the figures F has been scaled-down by 300 and F_{SA} has been normalized by a factor of 30 so as to display them in the same scale as the density matrix elements. We see that the SA-QFI again faithfully captures the expected sensitivity to small changes in g indicated by the changes in the density matrix elements when compared to the regular QFI.

in the peak of SA-QFI shifting to the right for larger g and also in the additional inflection point that appears in the graph of SA-QFI. While initializing the state of the probe in $|e\rangle$ is not the best choice for improving the measurement sensitivity, considering this scenario makes a stronger case for using SA-QFI instead of QFI for determining the optimal measurement time in noisy quantum metrology schemes.

D. Dephasing

We explore the utility of SA-QFI in noisy metrology by considering a case where the noise does to take the state of the quantum probe outside the qubit subspace. In Fig. 4 we show the time dependence of the QFI and SA-QFI when the only noise acting on our system is the dephasing described by the operator $L_{ph} = |f\rangle\langle f| - |e\rangle\langle e|$. In this case there is no decay to the sink state and the

QFI, F and modified QFI, F_{SA} overlap with each other since $\rho_{ee} + \rho_{ff} = 1$ at all times as expected. Significantly, QFI maxima occur at locations where the probabilities of the states are rapidly changing.

E. QFI with respect to detuning

Finally we also explore the time dependence of the quantum Fisher information corresponding to the detuning parameter Δ in Fig. 5. The system here is initialized in the state $|f\rangle$ with L_e as the collapse operator. As in the case of estimation of g , here too we can see that the location of the peak in the SA-QFI reflects the dynamics and expected sensitivity of the open quantum probe faithfully compared to the standard QFI.

It should be noted here that while we have illustrated the QFI calculations for our model system with particular choices of γ_e and g , our results scale in a straightforward

F. An experiment to estimate g

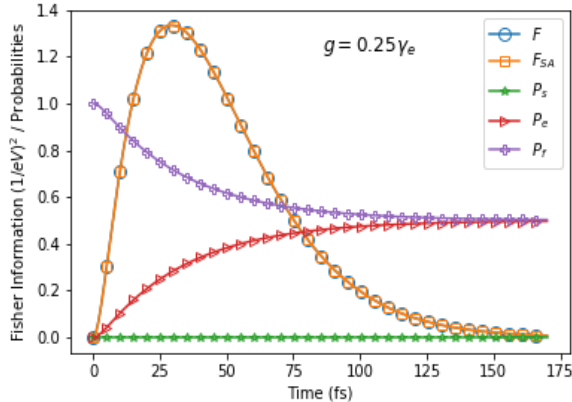


FIG. 4. The QFI, F and SA-QFI, F_{SA} for the case where the collapse operator is the dephasing operator $L_{ph} = |f\rangle\langle f| - |e\rangle\langle e|$. The initial state is $|f\rangle$ and the parameter values used are: $\hbar\gamma_{ph} = 0.150\text{eV}$, $\hbar\gamma_{ph} = 0.0\text{eV}$ and $\hbar\Delta = 0.0\text{eV}$. Also shown are ρ_{ee} , ρ_{ff} and ρ_{ss} . F and F_{SA} have been scaled down by a factor of 400 to fit in the figure. The QFI and SA-QFI coincide in this case since the noise does not take the system outside the qubit subspace.

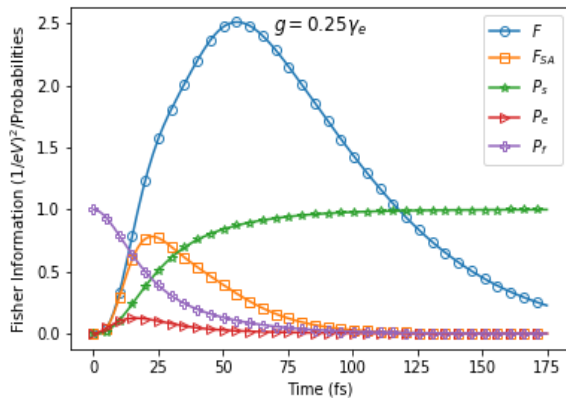


FIG. 5. The dependence of the QFI, F , and SA-QFI, F_{SA} , on the detuning parameter Δ corresponding to the initial state $|f\rangle$ is shown. The parameters used in the plots are: $\hbar\gamma_e = 0.150\text{eV}$, $g = \gamma_e/4$, $\hbar\Delta = 0.02\text{eV}$. Also shown are ρ_{ee} , ρ_{ff} and ρ_{ss} . Both F and F_N have been scaled down by a factor of 200 to fit in the figure. We see that for estimating Δ , also, F_{SA} serves as a better figure-of-merit for the expected performance of a noisy quantum probe.

manner to other cases. For example, with a fixed ratio of g/γ_e and the detuning parameter δ set to zero, the QFI magnitudes scale as $1/\gamma_e^2$, consistent with loss being detrimental and leading to smaller QFI values, and time scales approximately as γ_e , consistent with diminished loss leading to longer time scales.

Consider an experiment designed to estimate the parameter g . Atoms initialized in the state $|f\rangle$ pass through the cavity and then the number of atoms either in the state $|e\rangle$ or $|f\rangle$ is ascertained. The readout on the quantum probe is effected by the projection operator $\Pi_e = |e\rangle\langle e|$. Readout of the probe leads to a time dependent signal $\langle \Pi_e \rangle_t = \rho_{ee}(t)$, where $\rho_{ee}(t)$ is given in Eq. (11). The measured signal is a function of g and using $\langle \Pi_e \rangle$ as the estimator for g , we can obtain the value of the coupling with its variance given by

$$\Delta g(t) = \frac{\Delta \Pi_e(t)}{|d\langle \Pi_e \rangle_t / dg|}.$$

It is easy to see that since $\Pi_e^2 = \Pi_e$,

$$\Delta \Pi_e(t) = \rho_{ee}(t)(1 - \rho_{ee}(t)).$$

Let us consider the case in which $\alpha \rightarrow 0$ so that $\rho_{ee} = 4g^2 t^2 e^{-\gamma_e t/2}$ from Eq. (11) and we obtain,

$$\Delta^2 g(t) = \frac{g}{2} [1 - 4g^2 t^2 e^{-\gamma_e t/2}] \quad (13)$$

The quantum Cramer-Rao bound tells us that $\Delta^2 g(t) \geq 1/F$ where F is the quantum Fisher information. We see that $1/\Delta^2 g(t)$ has a maximum (and $\Delta^2 g(t)$ has a minimum) at $t = 4/\gamma_e = 1/g$. For the parameter values used in Fig. 1, the maximum of $1/\Delta^2 g(t)$ is at $t = 26.66\text{fs}$ which matches up closely with the peak of the SA-QFI rather than that of the QFI. We see that F_{SA} is a tighter and better bound on the achievable quantum Fisher information in possible experiments of the kind described above. Saturating the Fisher information depends on optimal choices for the initial state of the probe qubits as well as on optimizing the read-out procedure employed. Even without these optimisations it is clear that F_{SA} is operationally a better figure of merit for the performance of such metrology schemes in the presence of noise.

IV. NON-HERMITIAN APPROACH

We look at the noisy metrology scheme considered in the previous section again non-Hermitian quantum mechanics. In the non-Hermitian approach, the point $\alpha = 0$ corresponds to an exceptional point at which the non-Hermitian Hamiltonian transitions from being PT-symmetric to not being so. Comparison with the GKSL equation based analysis allows us to see clearly if the exceptional point can lead to advantages in quantum metrology. In the non-Hermitian approach we do not have to consider the sink state and the decay out of the state $|e\rangle$ at a rate γ_e can be described directly by adding a term proportional to $i|e\rangle\langle e|$ and modifying the Hamiltonian as

$$H_{\text{eff}} = H - i\hbar \frac{\gamma_e}{2} |e\rangle\langle e| = H - i \frac{\hbar}{2} L_e^\dagger L_e. \quad (14)$$

Note that H in Eq. (8) is made of only qubit operators and so is H_{eff} . We can therefore work entirely in the two dimensional qubit subspace spanned by states $|e\rangle$ and $|f\rangle$ in the non-Hermitian case. Furthermore, we can use state vectors to represent the probe state instead of density matrices and the probe state $|\psi_t\rangle$ evolves as,

$$i\hbar \frac{d|\psi_t\rangle}{dt} = H_{\text{eff}}|\psi_t\rangle. \quad (15)$$

Heuristically one can understand the connection between the GKSL approach and the non-Hermitian one by noting that in Eq. (9) the $L_e \rho L_e^\dagger$ term leads to a contribution proportional to $|s\rangle\langle s|$ in the master equation while the anti-commutator in Eq. (9) produces contributions proportional to $|e\rangle\langle e|$. The effect of the anti-commutator is captured by the non-Hermitian term that is introduced. A formal development of this connection can be found in [27].

We can represent the effective Hamiltonian, H_{eff} , by a 2×2 matrix,

$$H_{\text{eff}} = \hbar \begin{pmatrix} \Delta - i\frac{\gamma_e}{2} & g \\ g & \Delta \end{pmatrix} \quad (16)$$

The eigenvalues and eigenvectors of H_{eff} are,

$$\lambda_1 = \Delta + \frac{-i\gamma_e - \alpha}{4}, \quad |\Psi_1\rangle = \frac{1}{\sqrt{2}} \begin{pmatrix} \frac{-i\gamma_e - \alpha}{4g} \\ 1 \end{pmatrix} \quad (17)$$

and

$$\lambda_2 = \Delta + \frac{-i\gamma_e + \alpha}{4}, \quad |\Psi_2\rangle = \frac{1}{\sqrt{2}} \begin{pmatrix} \frac{-i\gamma_e + \alpha}{4g} \\ 1 \end{pmatrix} \quad (18)$$

where, once again we have defined, $\alpha \equiv \sqrt{16g^2 - \gamma_e^2}$. We can use these eigenvalues and eigenvectors to construct a state $|\psi_t^e\rangle$ which at $t = 0$ starts at $|e\rangle$. Such a state is given by,

$$|\psi_t^e\rangle = \frac{-2g}{\alpha} (e^{-i\lambda_1 t} |\Psi_1\rangle - e^{-i\lambda_2 t} |\Psi_2\rangle) \quad (19)$$

and $|\psi_0^e\rangle = |e\rangle = (1, 0)^T$. We can also construct a state that starts at the initial state $|f\rangle$,

$$|\psi_t^f\rangle = \frac{8\sqrt{2}g^2}{\alpha^2 + i\gamma_e\alpha} (e^{-i\lambda_1 t} |\Psi_1\rangle + B e^{-i\lambda_2 t} |\Psi_2\rangle) \quad (20)$$

where B is given by,

$$B = \frac{\alpha^2 - 8g^2 + i\gamma_e\alpha}{8g^2} \quad (21)$$

with $|\psi_0^f\rangle = |f\rangle = (0, 1)^T$. Let us specialize to the case where our initial state is $|f\rangle$. We can use the state $|\psi_t^f\rangle$ to calculate the quantum Fisher information using the pure state formula Eq. (7). We denote this QFI by Pure- $F_{2 \times 2}^{\text{NH}}$. This formula however will be incorrect since the derivation of Eq. (7) assumes the conservation of probabilities and clearly in our non-hermitian case the probabilities

are not conserved. We can also use this state to construct the density matrix,

$$\rho_{2 \times 2}^{\text{NH}} = |\psi_t^f\rangle\langle\psi_t^f| \quad (22)$$

We can use this density matrix in the mixed state QFI formula Eq. (5) to calculate Mixed- $F_{2 \times 2}^{\text{NH}}$ and as expected we find Pure- $F_{2 \times 2}^{\text{NH}} \neq$ Mixed- $F_{2 \times 2}^{\text{NH}}$ (see Fig. 6). Let us now extend our 2×2 density matrix to a 3×3 density matrix,

$$\rho_{3 \times 3}^{\text{NH}} = \begin{pmatrix} \rho_{2 \times 2}^{\text{NH}} & 0 \\ 0 & \rho_{ss} \end{pmatrix} \quad (23)$$

where $\rho_{ss} = (1 - \rho_{ee} - \rho_{ff})$. This density matrix is exactly the density matrix given in Eq. (11) and the QFI calculated with it Mixed- $F_{3 \times 3}^{\text{NH}}$ is therefore exactly the same as the QFI, F calculated earlier using the GKSL equation (see Fig. 6). The density matrix $\rho_{3 \times 3}^{\text{NH}}$ has three eigenvalues σ_1, σ_2 and σ_3 where σ_1 is non zero at all times, $\sigma_2 = 0$, and $\sigma_3 = \rho_{ss}$ due to the block diagonal form of the density matrix. The components of the QFI given in Eq. (6) that contribute to the total QFI, $F =$ Mixed- $F_{3 \times 3}^{\text{NH}}$ are $F(\sigma_1, \sigma_1)$, $F(\sigma_1, \sigma_2)$, $F(\sigma_2, \sigma_1)$ and $F(\sigma_3, \sigma_3)$.

An important point to note in Fig. 6 is that all the QFI's have been plotted at the exceptional point $\alpha = 0$ and we see no special behavior at that point. This further supports the point that operating a quantum probe at the exceptional point does not yield advantages in quantum metrology as previously pointed out in [21, 22].

V. SUBSPACE ADAPTED QFI VS POST-SELECTION

A three level system with identical configuration as the one we consider was studied experimentally in [13]. Three levels of a superconducting transmon qubit formed the states $|e\rangle$, $|f\rangle$ and $|s\rangle$ (labelled as $|g\rangle$ in [13]). States $|e\rangle$ and $|f\rangle$ are treated as the qubit levels in the experiment as well while the ground state of the transmon is the sink $|s\rangle$. The decay rate γ_e is controllable in the experiment and the focus of the study is the exceptional point that can be approached from either side by tuning γ_e . Experimental results are restricted to the qubit subspace by doing post-selection and choosing only those experimental runs in which the final state of the transmon is within the $|e\rangle - |f\rangle$ subspace. The post selection procedure results in normalized probabilities given by,

$$\bar{P}_f = \frac{\rho_{ff}}{\rho_{ff} + \rho_{ee}}, \quad \bar{P}_e = \frac{\rho_{ee}}{\rho_{ff} + \rho_{ee}} \quad (24)$$

with $\bar{P}_f = 1 - \bar{P}_e$.

The post-selection re-normalizes the probabilities for the transmon being in the qubit subspace. This allows for treating the qubit state as effectively pure and using the relation between QFI and the Bures distance [28]. For qubit states lying around the equator of the Bloch sphere ($\bar{P}_f \sim \bar{P}_e \sim 0.5$) the QFI is approximated by

$$\bar{F} \simeq \left(\frac{d\bar{P}_f}{dg} \right)^2.$$

The normalized probability \bar{P}_f shows very different behavior on either side of the exceptional point and because of this \bar{F} diverges around the exceptional point indicating the possibility of metrological advantage. Our analysis shows that the bare probability of the qubit being in state $|f\rangle$ changes smoothly across the exceptional point and the difference in behavior is limited to the post-selected and normalized probabilities.

It is pointed out clearly in [13] that the post selection comes with a cost and around the exceptional point, the post-selection efficiencies are very low. Advantages in quantum measurements, if any, furnished by working around the exceptional point therefore has to be tempered by clarity in counting the resources that went into the measurement scheme. If each use of the quantum probe is counted, then post-selection around the exceptional point is costly since almost all trials end up with the probe in the state $|s\rangle$ and the trial being discarded. In such a scenario the SA-QFI quantifies the maximum amount of information about the parameter that can be extracted per use of the probe with the additional restriction that only those probes whose final state is in the qubit subspace can carry any information about the parameter being measured. The optimal duration of the parameter dependent evolution of the probe is also determined by the SA-QFI. On the other hand, if each use of the quantum probe is not counted as a resource (or they are treated as a “free” resource) then there is a metrological advantage in working around the exceptional point as seen from the elegant experiments reported in [13].

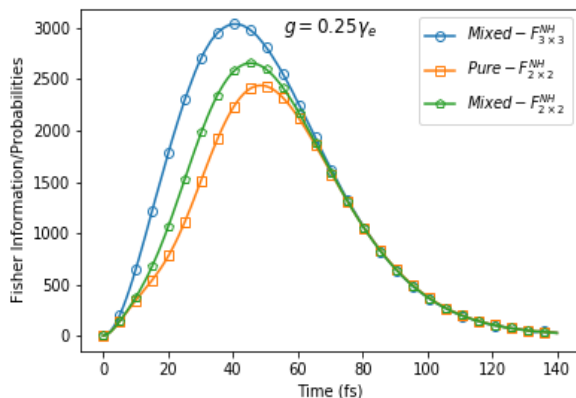


FIG. 6. The plot of QFI, Pure- $F_{2 \times 2}^{NH}$ calculated using the pure state vector $|\psi_t^f\rangle$, the QFI, Mixed- $F_{2 \times 2}^{NH}$ calculated using the density matrix $\rho_{2 \times 2}^{NH}$ and the QFI, Mixed- $F_{3 \times 3}^{NH}$ calculated using the density matrix $\rho_{3 \times 3}^{NH}$ vs time is provided. The plot is made at the exceptional point $\alpha = 0$.

VI. N-PROBES CASE

It is straightforward to generalize the single excitation manifold to the case of N qubits and a resonator mode.

See also [29]. Our Hamiltonian in this case can be written as,

$$H_{\text{eff}}^n = H_N - \frac{i\hbar\gamma_e}{2}|e\rangle\langle e| \quad (25)$$

where

$$H_N = \hbar g \sum_{i=1}^N (|e\rangle\langle f_i| + |f_i\rangle\langle e|) \quad (26)$$

and $|e\rangle = (1, 0, 0 \dots 0)^T$, $|f_1\rangle = (0, 1, 0 \dots 0)^T$, $|f_2\rangle = (0, 0, 1 \dots 0)^T$ and so on, are $(N + 1)$ - dimensional column vectors. We can use the Hamiltonian in Eq. (25) to compute the density matrix of the N qubits and the sink state as a function of time as,

$$\rho_{(N+1) \times (N+1)}^{NH}(t) = \begin{pmatrix} \rho_{N \times N}^{NH}(t) & 0 \\ 0 & \rho_{ss}(t) \end{pmatrix} \quad (27)$$

where $\rho_{ss} = 1 - \rho_{ee} - \sum_i \rho_{f_i f_i}$ as a straightforward generalization of the procedure followed in $N = 1$ case. We can then use this density matrix to calculate the QFI and SA-QFI for N probes. The definition of SA-QFI for a general N is,

$$F_{\text{SA}} = \left(\rho_{ee} + \sum_i \rho_{f_i f_i} \right) F \quad (28)$$

It is then of interest to examine how the QFI scales with increasing N since we know that in the standard quantum limit (SQL) the QFI should increase linearly with N and in the ultimate Heisenberg limit it should scale quadratically with N [30]. We study the scaling of the maximum value of the QFI for three different initial states, $|e\rangle + |\chi\rangle$, $|\chi\rangle$ and $|f_1\rangle$ in Figs. 7 and 8. We see that for the states $|e\rangle + |\chi\rangle$ and $|\chi\rangle$ the peak of the QFI does increase as one increases the N . However, as noted in the figure caption, these increases appear to be sublinear, i.e., does not even reach the SQL. We also see from Figs. 7 and 8 that, for the $|f_1\rangle$ state, the QFI actually decreases with increasing N . Thus for the three particular initial states examined we see that the effect of loss appears to be detrimental to even achieving the SQL, let alone the Heisenberg limit. This seems to be a feature of the fact that we are in 1-excitation manifold and the initial states we can have are the ones with very small amount of entanglement.

Above we studied the scaling of the QFI and SA-QFI numerically but for some special cases some analytical insight can also be obtained. Consider transforming to the basis composed of the states $|e\rangle$,

$$|\chi_1\rangle = \frac{1}{\sqrt{N}} \sum_i |f_i\rangle, \quad (29)$$

and $N - 1$ states $|\chi_2\rangle, |\chi_3\rangle \dots |\chi_N\rangle$ that are orthogonal to $|e\rangle$ and $|\chi_1\rangle$ for the N -qubit Hamiltonian, Eq. (25). In this new basis the dynamics with the single excitation manifold is fully described by a 2×2 sub-block of the

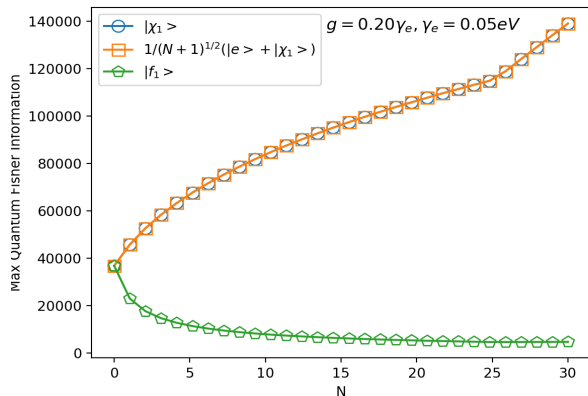


FIG. 7. The maximum value of the quantum Fisher information is plotted against N . We see that the maximum value of the QFI decreases for the state $|f\rangle$ with increasing N and scales as $N^{-0.69}$. The maximum QFI for the initial state $|\chi_1\rangle$ and $|e\rangle + |\chi_1\rangle$ increases with N and scales as $N^{0.52}$ till $N = 25$ after which it achieves the SQL and becomes linear with N .

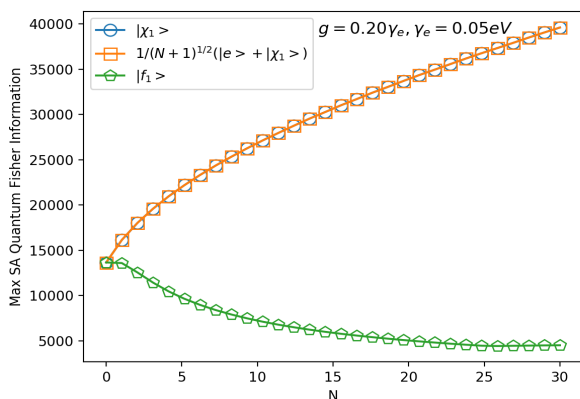


FIG. 8. The maximum value of the subspace adapted quantum Fisher information is plotted against N . We see that the maximum value of the SA-QFI also decreases for the state $|f\rangle$ with increasing N just like it does for QFI and scales as $N^{-0.30}$. The maximum SA-QFI for the initial states $|\chi_1\rangle$ and $|e\rangle + |\chi_1\rangle$ increases with N and scales as $N^{0.67}$.

Hamiltonian as shown in the appendix Eq. (34). See also Ref. [31]. We can see that in this effective two dimensional sub-space the coupling scales as $\sqrt{N}g$. This shows the equivalence of the N -qubit model with coupling g to an $N = 1$ model with coupling $\sqrt{N}g$. Of course this is not surprising because our model is a variation on the Tavis-Cummings model [32, 33]. Therefore if we choose the initial state to be $|\chi_1\rangle$ we obtain the following relationship between the QFI's of the N -qubit model and the single qubit model,

$$F(N, g, \chi_1) = NF(1, \sqrt{N}g, \chi_1). \quad (30)$$

The origin of the pre-factor N in the above equation is the square of the derivative with respect to g of the density matrix coming from the QFI formula. If, on the other hand, we choose the initial state to be $|f_1\rangle$, the norm of this state is equivalent to $1/N$ which shows up in the density matrix and cancels the pre-factor in the above equation and we get,

$$F(N, g, f_1) = F(1, \sqrt{N}g, f_1). \quad (31)$$

We can easily see from Fig. 1 that the QFI for $N = 1$ decreases with increasing g and since in the above formula the effective coupling is $\sqrt{N}g$, the function $F(1, \sqrt{N}g)$ will decrease with increasing N . In Fig. 7 we also see that after $N = 25$ the maximum QFI becomes a linear function of N for the initial states $|\chi_1\rangle$ and $|e\rangle + |\chi_1\rangle$ and we achieve the SQL limit. When N becomes larger, the effective coupling $\sqrt{N}g$ appearing in Eq. (30) grows while the rate of decay γ_e within the single excitation manifold remains unchanged. For large values of the effective coupling, losses are therefore practically negligible and we get back the noiseless case. This is reflected in the second and subsequent peaks of the QFI growing and becoming larger than the first peak indicating that information about the measured parameter continues to be available even after the qubit populations have gone through several rounds of oscillations between the ground state and singly excited state. Both Eqs. (30) and (31), as well as an associated one for starting with all basis components excited are derived in the Appendix.

VII. CONCLUSIONS AND FUTURE DIRECTIONS

The quantum Fisher information is an important tool for characterizing quantum sensing and metrology and it bounds the accuracy with which a parameter can be estimated using a measurement scheme that uses quantum probes. In this work we studied the time-dependent quantum Fisher information for an atom-cavity open quantum system and focused on estimating the coupling g of the atom with the cavity. Due to there being losses in the system we find that the time-dependent quantum Fisher information has a peak value in time, suggesting that there is an optimal point in time where the quantum measurements should be performed to obtain the best possible estimate of g . However, upon closer monitoring of the dynamics of the system, i.e. monitoring the probabilities of the probe being in various states and the rates of change of these probabilities, it was found that the peak of the QFI does not align with the location in time where the system has rapid, parameter dependent dynamics and thus is expected to be most sensitive to g . We have therefore proposed a modified definition of the QFI called the subspace adapted QFI which more accurately captures the dynamics of the system and suggests an optimal time at which to perform the quantum

measurements to yield the best possible measurement accuracy.

Our analysis involved computing the time evolution of the density matrix of probe system and cavity which we calculated using the GKSL master equation. We also studied our model via the non-hermitian formalism and showed how a naive application of the QFI formulae here give inaccurate results. We then provided a method of extending the non-hermitian formalism such that its results match with what we obtain from the GKSL formalism. An interesting aside of this study was that there is nothing special happening at the so-called exceptional points in terms of the behavior of the QFI which corroborates with earlier studies [21, 22].

One strategy to deal with quantum metrology in open quantum systems is to do post-selection. This strategy involved counting only the measurements that are within the experimentally accessible subspace. We provide reasons why the strategy of performing measurements at an optimal time guided by the subspace adapted QFI might be more appropriate particularly when each use of the quantum probe has to be treated as a resource that is utilized for the measurement irrespective of whether the trial survives the post-selection or not.

Lastly we studied the scaling of the QFI and SA-QFI with the number of atoms in our quantum system when limited to the manifold of singly excited states. Here we find that the losses have a very detrimental effect and does not allow the measurement to even achieve the standard quantum limit (SQL). The variety of initial states within the single excitation manifold that we tried were limited and it is possible that a more appropriate choice of initial state can help in achieving the SQL and maybe even saturate the Heisenberg limit. However, we leave this question for future investigations. Since we restricted ourselves to the single excitation manifold, the amount of entanglement that the initial states can have is also limited possibly leading to measurement accuracies that are worse than the SQL. It is very likely that going to higher excitation manifolds will help us breach the SQL barrier and it may be possible go closer to the Heisenberg limit. However the detrimental effects of the noise are likely to be amplified as well in this case. In our work, we have also found for the first time mathematical expressions relating the QFI for the case with a single probe qubit ($N = 1$) with the QFI for the case of N probes restricted to the single excitation manifold. Exploring similar relations in the presence of multiple excitation is left as a question to be taken up in the future.

ACKNOWLEDGMENTS

This material is based upon work supported by the U.S. Department of Energy Office of Science National Quantum Information Science Research Centers. Work performed at the Center for Nanoscale Materials, a U.S. Department of Energy Office of Science User Facility, was

supported by the U.S. DOE Office of Basic Energy Sciences, under Contract No. DE-AC02-06CH11357. Z.H.S would like to thank Michael Perlin for helpful discussions. A. S. was supported by QuEST grant No Q-113 of the Department of Science and Technology, Government of India.

APPENDIX

The matrix representation of our Hamiltonian Eq. (25) in the $|e\rangle, |f_1\rangle, |f_2\rangle, \dots$ basis. is given by

$$H = \hbar \begin{pmatrix} -i\frac{\gamma_e}{2} & g & g & \dots \\ g & 0 & 0 & \dots \\ g & 0 & 0 & \dots \\ \vdots & \vdots & \vdots & \ddots \end{pmatrix} \quad (32)$$

Let us transform to new orthogonal basis $|e\rangle, |\chi_1\rangle, |\chi_2\rangle, \dots$, where $|\chi_1\rangle$ is given by

$$|\chi_1\rangle = \frac{1}{\sqrt{N}} \sum_i |f_i\rangle. \quad (33)$$

By construction, $|e\rangle$ and $|\chi_1\rangle$ are orthogonal. We can find the remaining $|\chi_2\rangle, |\chi_3\rangle, \dots, |\chi_N\rangle$ basis states that are orthogonal to $|e\rangle$ and $|\chi_1\rangle$ via a Gram-Schmidt procedure applied to $|f_2\rangle, \dots, |f_N\rangle$, for example. In this new basis the matrix representation of our Hamiltonian is given by

$$H = \hbar \begin{pmatrix} H_{2 \times 2} & 0 & \dots \\ 0 & 0 & \dots \\ \vdots & \vdots & \ddots \end{pmatrix}, \quad H_{2 \times 2} = \begin{pmatrix} -i\frac{\gamma_e}{2} & \sqrt{N}g \\ \sqrt{N}g & 0 \end{pmatrix} \quad (34)$$

Now the Hamiltonian matrix in this basis is effectively a 2×2 block involving the $|e\rangle$ state and the $|\chi_1\rangle$ state above, with coupling $\sqrt{N}g$. This shows that the N -atom Hamiltonian with coupling g can be essentially described by a $N = 1$ Hamiltonian with a $\sqrt{N}g$ coupling between its two states. For a related treatment, see Ref. 31.

It is now possible to write down exact expressions for the time evolved density matrix and the quantum Fisher information all in terms of the solution of the 2×2 problem. Given the block diagonal structure of our Hamiltonian, Eq. (34), our density matrix $\rho(t)$ will also have a block diagonal structure in the new basis,

$$\rho(t) = \begin{pmatrix} \rho_{ee} & \rho_{e1} & 0 & 0 & 0 & \dots \\ \rho_{1e} & \rho_{11} & 0 & 0 & 0 & \dots \\ 0 & 0 & \rho_{22} & 0 & 0 & \dots \\ 0 & 0 & 0 & \rho_{33} & 0 & \dots \\ \vdots & \vdots & \vdots & \vdots & \ddots & \dots \end{pmatrix}, \quad (35)$$

where the indices 1, 2, \dots , N refer to $|\chi_1\rangle, |\chi_2\rangle, \dots, |\chi_N\rangle$. A general initial condition in the original basis $|e\rangle, |f_1\rangle, |f_2\rangle, \dots$ will have the form,

$$|\psi(0)\rangle = a_e |e\rangle + \sum_{k=1}^N a_k |\chi_k\rangle \quad (36)$$

in the $|e\rangle, |\chi_1\rangle, |\chi_2\rangle \dots$ basis. The density matrix elements $\rho_{22}, \rho_{33}, \dots$ will be constant in time. If we define the re-scaled coupling to be $G = \sqrt{N}g$ for the $H_{2 \times 2}$, we have $d\rho_{kk}/dG = 0$ for all $k = 2, 3, \dots$. For the density matrix elements that are not constant, we have,

$$\frac{d\rho}{dg} = \sqrt{N} \frac{d\rho}{dG} \quad (37)$$

Since the general form of the quantum Fisher information, Eqs. (5) and (6), involves derivatives with respect to g (or G), the quantum Fisher information inferred from just the upper 2×2 part of Eq. (35) (along with any auxiliary quantities such as ρ_{ss} discussed below) will be the quantum Fisher information for the full problem. Since the square of the density matrix with respect to g is what enters the quantum Fisher information formula,

$$\left(\frac{d\rho}{dg}\right)^2 = N \left(\frac{d\rho}{dG}\right)^2,$$

it is clear that, for some initial condition $|\psi(0)\rangle$,

$$F(N, g, \psi(0)) = N F(1, G = \sqrt{N}g, \psi(0)), \quad (38)$$

This means that the N qubit quantum Fisher information with coupling g can be obtained from an $N = 1$ qubit quantum Fisher information with coupling $G = \sqrt{N}g$ based on the 2×2 , $|e\rangle - |\chi_1\rangle$ subspace and with an appropriate initial condition, $a_e(0), a_1(0)$ (inferred from $\psi(0)$). In addition to the factor of N on the right-hand side of Eq. (38), there can be additional N dependence arising from the initial state employed. Let us analyze several initial states.

- $|\psi(0)\rangle = \frac{1}{\sqrt{N}} \sum_i |f_i\rangle = |\chi_1\rangle$: In this case we have $a_e = \langle e|\psi(0)\rangle = 0$ and $a_1 = \langle \chi_1|\psi(0)\rangle = 1$ and therefore no extra N dependence is introduced in the Eq. (38).
- $|\psi(0)\rangle = |f_1\rangle$: For this initial state $a_e = \langle e|\psi(0)\rangle = 0$ and $a_1 = \langle \chi_1|\psi(0)\rangle = 1/\sqrt{N}$. We will therefore have to solve our 2×2 system with this initial condition which overall has norm $1/N$ instead of unity. We could equivalently solve the 2×2 system with initial condition $a_e = 0$ and $a_1 = 1$, and multiply the overall result by $1/N$. In the latter case this factor will cancel the prefactor on the right hand side in the Eq. (38).
- $|\psi(0)\rangle = \frac{1}{\sqrt{N+1}}(|e\rangle + \sum_i |f_i\rangle)$: For this initial condition, $a_e = \langle e|\psi(0)\rangle = 1/\sqrt{N+1}$ and $a_1 = \langle \chi_1|\psi(0)\rangle = \sqrt{N/(N+1)}$. Notice here that while $|e\rangle$ and all the $|f_i\rangle$ have equal amplitudes in the original basis, $|e\rangle$ and $|a_1\rangle$ are not equally weighted. As with the first example, the pre-factor of N in Eq. (38) will remain in tact.

In the formula for $F(1, G = \sqrt{N}g, \psi(0))$ the density matrix elements $\rho_{ee}, \rho_{1e}, \rho_{e1}$ and ρ_{11} contribute. However our open quantum system has a sink state as well. The density matrix element ρ_{ss} corresponding to the sink state can be calculated via $\rho_{ss}(t) = 1 - \rho_{ee}(t) - \rho_{11}(t) - \rho_{22}(t) - \dots - \rho_{NN}(t)$. We will therefore have to lift our 2×2 density matrix to the 3×3 density matrix as given in Eq. (23) to calculate $F(1, G = \sqrt{N}g, \psi(0))$.

-
- [1] H. Cramér, A contribution to the theory of statistical estimation, *Scandinavian Actuarial Journal* **1946**, 85 (1946).
 - [2] C. R. Rao, Information and the accuracy attainable in the estimation of statistical parameters, in *Breakthroughs in statistics* (Springer, 1992) pp. 235–247.
 - [3] R. A. Fisher, On the mathematical foundations of theoretical statistics, *Philosophical transactions of the Royal Society of London. Series A, containing papers of a mathematical or physical character* **222**, 309 (1922).
 - [4] S. L. Braunstein and C. M. Caves, Statistical distance and the geometry of quantum states, *Physical Review Letters* **72**, 3439 (1994).
 - [5] V. Giovannetti, S. Lloyd, and L. Maccone, Quantum-Enhanced Measurements: Beating the Standard Quantum Limit, *Science* **306**, 1330 (2004).
 - [6] C. L. Degen, F. Reinhard, and P. Cappellaro, Quantum sensing, *Reviews of modern physics* **89**, 035002 (2017).
 - [7] D. Braun, G. Adesso, F. Benatti, R. Floreanini, U. Marzolino, M. W. Mitchell, and S. Pirandola, Quantum-enhanced measurements without entanglement, *Reviews of Modern Physics* **90**, 035006 (2018), publisher: American Physical Society.
 - [8] L. Pezzè, A. Smerzi, M. K. Oberthaler, R. Schmied, and P. Treutlein, Quantum metrology with nonclassical states of atomic ensembles, *Reviews of Modern Physics* **90**, 035005 (2018), publisher: American Physical Society.
 - [9] V. Giovannetti, S. Lloyd, and L. Maccone, Quantum metrology, *Physical review letters* **96**, 010401 (2006).
 - [10] V. Giovannetti, S. Lloyd, and L. Maccone, Advances in quantum metrology, *Nature Photonics* **5**, 222 (2011).
 - [11] M. Barbieri, Optical Quantum Metrology, *PRX Quantum* **3**, 010202 (2022), publisher: American Physical Society.
 - [12] M. Aspelmeyer, T. J. Kippenberg, and F. Marquardt, Cavity optomechanics, *Reviews of Modern Physics* **86**, 1391 (2014).
 - [13] M. Naghiloo, M. Abbasi, Y. N. Joglekar, and K. W. Murch, Quantum state tomography across the exceptional point in a single dissipative qubit, *Nature Physics* **15**, 1232 (2019), number: 12 Publisher: Nature Publishing Group.
 - [14] E. Polino, M. Valeri, N. Spagnolo, and F. Sciarrino, Photonic quantum metrology, *AVS Quantum Science* **2**, 024703 (2020).
 - [15] V. Gorini, A. Kossakowski, and E. C. G. Sudarshan,

- Completely positive dynamical semigroups of N-level systems, *Journal of Mathematical Physics* **17**, 821 (1976), publisher: American Institute of Physics.
- [16] G. Lindblad, On the generators of quantum dynamical semigroups, *Communications in Mathematical Physics* **48**, 119 (1976).
- [17] D. Chruściński and S. Pascazio, A Brief History of the GKLS Equation, *Open Systems & Information Dynamics* **24**, 1740001 (2017).
- [18] D. Manzano, A short introduction to the lindblad master equation, *Aip Advances* **10**, 025106 (2020).
- [19] Y. Ashida, Z. Gong, and M. Ueda, Non-hermitian physics, *Advances in Physics* **69**, 249 (2020).
- [20] C. M. Bender, S. Boettcher, and P. N. Meisinger, Ptsymmetric quantum mechanics, *Journal of Mathematical Physics* **40**, 2201 (1999).
- [21] H.-K. Lau and A. A. Clerk, Fundamental limits and non-reciprocal approaches in non-hermitian quantum sensing, *Nature communications* **9**, 1 (2018).
- [22] W. Langbein, No exceptional precision of exceptional-point sensors, *Physical Review A* **98**, 023805 (2018).
- [23] A. S. Holevo, *Probabilistic and statistical aspects of quantum theory*, Vol. 1 (Springer Science & Business Media, 2011).
- [24] C. W. Helstrom, Quantum detection and estimation theory, *Journal of Statistical Physics* **1**, 231 (1969).
- [25] J. Liu, H. Yuan, X.-M. Lu, and X. Wang, Quantum fisher information matrix and multiparameter estimation, *Journal of Physics A: Mathematical and Theoretical* **53**, 023001 (2019).
- [26] W. Chen, M. Abbasi, Y. N. Joglekar, and K. W. Murch, Quantum jumps in the non-hermitian dynamics of a superconducting qubit, *Physical Review Letters* **127**, 140504 (2021).
- [27] K. G. Zloshchastiev and A. Sergi, Comparison and unification of non-Hermitian and Lindblad approaches with applications to open quantum optical systems, *Journal of Modern Optics* **61**, 1298 (2014).
- [28] D. Bures, An extension of kakutani's theorem on infinite product measures to the tensor product of semifinite w*-algebras, *Transactions of the American Mathematical Society* **135**, 199 (1969).
- [29] C. L. Cortes, M. Otten, and S. K. Gray, Non-hermitian approach for quantum plasmonics, *The Journal of Chemical Physics* **152**, 084105 (2020).
- [30] S. Boixo, S. T. Flammia, C. M. Caves, and J. M. Geremia, Generalized Limits for Single-Parameter Quantum Estimation, *Phys. Rev. Lett.* **98**, 090401 (2007).
- [31] J. A. Campos-Gonzalez-Angulo and J. Yuen-Zhou, Generalization of the Tavis-Cummings model for multi-level anharmonic systems: Insights on the second excitation manifold, *J. Chem. Phys.* **156**, 194308 (2022).
- [32] M. Tavis and F. W. Cummings, Exact solution for an N-molecule-radiation-field hamiltonian, *Physical Review* **170**, 379 (1968).
- [33] B. M. Garraway, The Dicke model in quantum optics: Dicke model revisited, *Phil. Trans. R. Soc. A* **369**, 1137 (2011).